

# Chiral Bound States from Berry Curvature and Chiral Superconductivity

Daniil Karuzin,<sup>1</sup> Zhiyu Dong,<sup>2</sup> and Leonid Levitov<sup>3</sup>

<sup>1</sup>*Moscow Institute of Physics and Technology, Dolgoprudny 141701, Russia*<sup>\*</sup>

<sup>2</sup>*Department of Physics, California Institute of Technology, Pasadena CA 91125*

<sup>3</sup>*Department of Physics, Massachusetts Institute of Technology, Cambridge MA02139, USA*<sup>†</sup>

Motivated by the discovery of exotic superconductivity in rhombohedral graphene, we study the two-body problem in electronic bands endowed with Berry curvature and show that it supports chiral, non- $s$ -wave bound states with nonzero angular momentum. In the presence of a Fermi sea, these interactions give rise to a chiral pairing problem featuring multiple superconducting phases that break time-reversal symmetry. These phases form a cascade of chiral topological states with different angular momenta, where the order-parameter phase winds by  $2\pi m$  around the Fermi surface, with  $m = 1, 3, 5, \dots$ , and the succession of phases is governed by the Berry-curvature flux through the Fermi-sea area,  $\Phi = bk_F^2/2$ . As  $\Phi$  increases, the system undergoes a sequence of first-order phase transitions between distinct chiral phases, occurring nearly periodically in  $\Phi$  with period two. This realizes a quantum-geometry analog of the Little-Parks effect—oscillations in  $T_c$  that provide a clear and experimentally accessible hallmark of chiral superconducting order.

Since its inception, graphene has been widely explored as a platform for exotic superconductivity [1–6, 13]. Over the past several years, this idea has been put on solid footing, first by the discovery of superconductivity in twisted bilayer graphene [7–11, 22] and, more recently, by the observation of a variety of correlated states that spontaneously break time-reversal symmetry in rhombohedral graphene [14–24]. Most recently, direct signatures of chiral superconductivity have been reported in rhombohedral graphene tetralayer and pentalayer [25], followed by a flurry of theoretical work probing various aspects of time-reversal-symmetry-breaking superconductivity, including the effects of Berry phase and unconventional pairing mechanisms [35–52].

The main idea of this work is that, rather than focusing on specific microscopic pairing mechanisms—a direction actively pursued in the literature—we consider a general pairing interaction and explore the consequences of the geometric phase acquired by Cooper pairs upon scattering, a universal effect present for any pairing interaction, regardless of its microscopic origin. This perspective clarifies the relation between the pairing problem and the quantum-geometry problem of two-particle bound states, which turns out to be quite illuminating. In particular, the paired states exhibit a cascade of chiral phases controlled by the commensurability between the Berry-curvature flux and the Fermi-sea area, as illustrated in Fig. 1, while the corresponding two-body bound states show a very different behavior (Fig. 2).

We develop a microscopic framework for this physics using a simple, exactly solvable model of a single band with Berry phase. The resulting phase diagram features a sequence of chiral paired phases with related topological properties, and first-order transitions between these phases give rise to a “quantum-geometric” Little-Parks

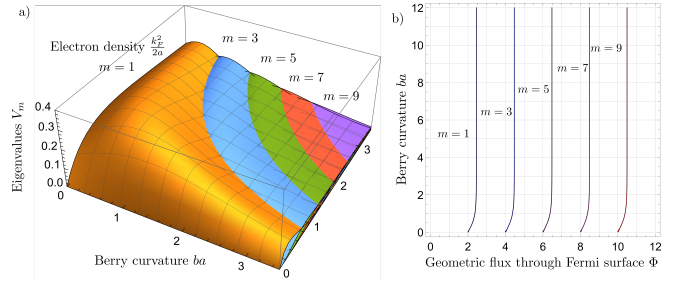


FIG. 1. (a) Hierarchy of chiral pairing channels for the chiral two-body interaction, Eq. (4), controlled by the Berry-curvature flux  $\Phi$ , Eq. (23), and the Fermi-sea area. Shown are eigenvalues of the linearized gap equation, Eq. (12), versus Berry curvature  $b$  and carrier density  $k_F^2/4\pi$ , measured in units of  $1/a$  and  $a/2\pi$ , respectively. The 3D surfaces show the leading eigenvalues, labeled by angular momentum  $m = 1, 3, 5, 7, \dots$ . Phase boundaries  $V_m = V_{m+2}$  between chiral phases with different  $m$  are well approximated by the hyperbolae  $bk_F^2/2 = \sqrt{(m+1)(m+2)}$ . (b) The same phase boundaries  $V_m = V_{m+2}$  in terms of flux  $\Phi$ , occurring near integer  $\Phi$  at small  $b$  and near half-integer  $\Phi$  at large  $b$ . Their periodicity in  $\Phi$  is captured by the Ginzburg–Landau energy local on the Fermi circle, Eq. (28), which predicts first-order transitions and Little-Parks-type oscillations with period  $\Delta\Phi = 2$ .

like effect, manifesting as oscillations of the critical temperature  $T_c$  as a function of the Berry-phase flux through the Fermi sea.

It is instructive to draw a comparison with conventional type-II superconductors, where vortices induced by magnetic fields do not fundamentally alter the microscopic structure of the paired state; their main effect is to generate vortex phases and impact the long-range order of the system [26–30]. By contrast with the conventional case, Berry curvature directly influences pairing type and symmetry on microscales. Berry-curvature-induced pseudomagnetic fields also drive transitions between distinct topological superconducting phases, in which the order-parameter phase winds in momentum space and the superconducting state acquires nontrivial topology [45, 53–55]. Such phases are expected to exhibit strong orbital

\* also: Landau Institute for Theoretical Physics, Moscow, Russia

† email: levitov@mit.edu

magnetism, host exotic (Majorana) quasiparticles and chiral edge excitations, and display anomalous thermal transport and related signatures [53–56]. The goal of this work is to elucidate how Berry curvature reshapes the phase diagram of superconductors, promoting chiral, time-reversal-breaking states even in the absence of any applied magnetic field.

To understand the key aspects of the chiral pairing problem, we first consider the two-body problem

$$H_{12} = \frac{\mathbf{k}_1^2}{2m} + \frac{\mathbf{k}_2^2}{2m} + V(\mathbf{R}_1 - \mathbf{R}_2), \quad \mathbf{R}_j = \mathbf{r}_j + \mathbf{a}(\mathbf{k}_j), \quad (1)$$

where  $\mathbf{a}(\mathbf{k}) = i\langle u_{n\mathbf{k}} | \nabla_{\mathbf{k}} u_{n\mathbf{k}} \rangle$  is the Berry connection of band  $n$ , and we set  $\hbar = 1$ . The operators  $\mathbf{R}_j$  denote covariant particle coordinates [31–34]. This Hamiltonian can be viewed as the single-band projection of an underlying multiband Dirac-type Hamiltonian, where the covariant-derivative structure  $\mathbf{R}_i = i\partial_{\mathbf{k}_i} + \mathbf{a}(\mathbf{k}_i)$  emerges within the adiabatic approximation.

We stress that such quantum-geometry structure of the interaction is totally general, applicable to any band dispersion and any Berry connection distribution in  $k$  space, applicable both for the ordinary case when time reversal symmetry (TRS) is unbroken and when it is broken by valley polarization (this paper). TRS imposes the relation  $\mathbf{a}_K(\mathbf{k}) = -\mathbf{a}_{K'}(-\mathbf{k})$  between the Berry connections in the  $K$  and  $K'$  valleys. As a first step toward analyzing superconductivity in valley-polarized graphene (discussed below), we now consider two interacting electrons in the same valley.

We focus on the simplest case of a cylindrically symmetric interaction  $V(\mathbf{R}_1 - \mathbf{R}_2)$ , for which each angular-momentum channel can be solved exactly. Using translation symmetry, we work in momentum space,  $\mathbf{p}_j \rightarrow \hbar\mathbf{k}_j$ ,  $\mathbf{r}_j \rightarrow i\partial_{\mathbf{k}_j}$ ,  $j = 1, 2$ , and go to the center-of-mass frame by introducing relative coordinates and momenta:

$$\mathbf{r} = \mathbf{r}_1 - \mathbf{r}_2, \quad \mathbf{k} = (\mathbf{k}_1 - \mathbf{k}_2)/2. \quad (2)$$

The two-particle Hamiltonian in the center of mass frame  $\mathbf{k}_1 + \mathbf{k}_2 = 0$  takes the form of a one-particle Hamiltonian for a particle with a reduced mass  $\mu = m/2$ :

$$H_{12} = \frac{\hbar^2 \mathbf{k}^2}{2\mu} + V(\mathbf{R}_1 - \mathbf{R}_2), \quad \mathbf{R}_j = i\partial_{\mathbf{k}_j} + \mathbf{a}(\mathbf{k}_j). \quad (3)$$

To simplify algebra, below we specialize to the pairing interaction of a Gaussian form

$$V(\mathbf{R}_1 - \mathbf{R}_2) = \lambda e^{-a(\mathbf{R}_1 - \mathbf{R}_2)^2}, \quad \lambda < 0, \quad (4)$$

and choose Berry connection describing a uniform field

$$\mathbf{a}(\mathbf{k}) = \frac{bk}{2} \mathbf{e}_\varphi = \frac{1}{2}b(k_y, -k_x). \quad (5)$$

In this case, the chiral two-particle problem can be solved in a closed form. To that end, we consider the operator

$$\mathbf{R}^2 = \left( i\partial_{\mathbf{k}} + \frac{bk}{2} \mathbf{e}_\varphi \right)^2. \quad (6)$$

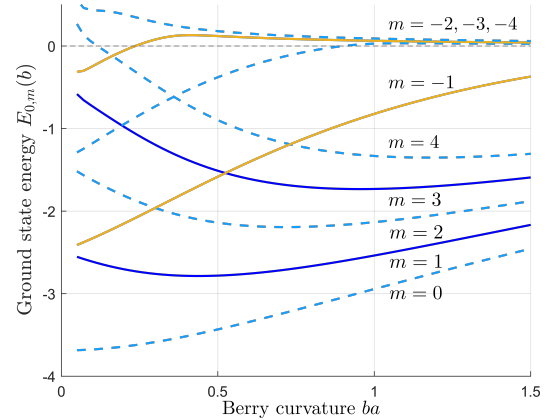


FIG. 2. Ground-state energies of the two-body problem, Eq. (1), as functions of  $b$  for different angular-momentum sectors  $m$ . Solid lines show odd  $m$  and dashed lines show even  $m$  for representative parameters. For fermions, even- $m$  and odd- $m$  channels correspond to spin-singlet and spin-triplet states, respectively. States with  $m$  and  $-m$  are degenerate at  $b = 0$  but become nondegenerate at finite  $b$ . Finite Berry curvature favors  $m > 0$  states, whose energies decrease (become more negative) as  $b$  increases. The apparent bound states at  $E > 0$  are a finite-size effect. Notably, the ground states with different  $m$  do not alternate as  $b$  varies, indicating that the alternation of pairing channels in Fig. 1 instead arises from geometric flux and the Fermi-sea area commensurability (see Eq. (28) and discussion).

This quantity is nothing but the Hamiltonian of a non-relativistic particle in an external magnetic field, with eigenvalues  $\rho_{n,m} = b(2n + |m| + m + 1)$ . The spectrum of the problem  $V(\mathbf{R})|\psi\rangle = \epsilon|\psi\rangle$  is therefore

$$\epsilon_{n,m} = \lambda e^{-a\rho_{n,m}}, \quad n \geq 0, \quad m = 0, \pm 1, \pm 2, \dots, \quad (7)$$

and the corresponding eigenfunctions in momentum space can be written as

$$\psi_{n,m}(k, \varphi) = ce^{-im\varphi} e^{-\frac{bk^2}{4}} k^{|m|} {}_1F_1\left(-n, |m| + 1, \frac{bk^2}{2}\right),$$

where  ${}_1F_1$  denotes a confluent hypergeometric function, and  $c = b^{\frac{1+|m|}{2}} \sqrt{\frac{(|m|+n)!}{\pi 2^{|m|+1} n! |m|!}}$  is normalization factor.

The Hamiltonian in Eq. (3), owing to its cylindrical symmetry, decomposes into independent blocks labeled by angular momentum  $m$ . In each  $m$ -sector, it can be represented in the circular basis  $\psi_{n,m}$  as a real symmetric tridiagonal matrix (here  $n, n' \geq 0$  and  $m$  is arbitrary):

$$\langle n' | H_{12}^{(m)} | n \rangle = g_n \delta_{n'n} + \tilde{g}_n \delta_{n',n-1} + \tilde{g}_{n'} \delta_{n',n+1} \quad (8)$$

$$g_n = \lambda e^{-a\rho_{n,m}} + \frac{2n + |m| + 1}{\mu b}, \quad \tilde{g}_n = -\frac{\sqrt{n(n + |m|)}}{\mu b}.$$

Diagonalizing this Hamiltonian yields the ground states in each  $m$ -sector as functions of  $b$ , as shown in Fig. 2. Notably, the states with angular momenta  $m$  and  $-m$  split into pairs of nondegenerate levels that (initially) disperse linearly with  $b$ , one moving up and the other

down in energy, whereas the  $m = 0$  state remains the ground state for all  $b$ . As  $b$  increases, the energies of the positive- $m$  states become more negative, while the energies of the negative- $m$  states increase and eventually merge with the positive-energy continuum. In the continuum,  $H_{12}$  describes a chiral scattering problem that gives rise to chiral pairing and superconductivity.

The tendency of Berry curvature to favor nonzero-chirality states is key to understanding how chiral superconductivity emerges. However, as a comparison between Figs. 1 and 2 shows, the leading- $m$  superconducting channel cannot be inferred directly from the properties of the chiral bound states. The reason is that new effects arise in the presence of a Fermi surface, where the superconducting instability actually develops. In particular, superconductivity becomes sensitive to a commensurability condition between the Berry flux enclosed by the Fermi surface and the Fermi sea area. As we will see, this commensurability leads to Little-Parks-type oscillations that govern the succession of superconducting states with different  $m$ .

We now proceed to analyze superconductivity in a 2D Fermi sea with a quantum-geometric pairing interaction:

$$H = \int d^2x \psi^\dagger(x) \left( \frac{\mathbf{p}^2}{2m} - \epsilon_F \right) \psi(x) + \frac{1}{2} \iint d^2x_1 d^2x_2 \psi^\dagger(x_2) \psi^\dagger(x_1) V(\mathbf{R}_1 - \mathbf{R}_2) \psi(x_1) \psi(x_2), \quad (9)$$

taking fermions as spinless. For simplicity, we ignore spin and valley degrees of freedom. This framework is relevant for the rhombohedral graphene superconducting systems in which electrons are spin- and valley-polarized. Spin-triplet pairing mandates odd-parity angular momentum  $m$ , limiting possible  $m$  to odd values  $m = 1, 3, 5, \dots$ . The model can be readily extended to include spin.

In what follows, we analyze the scattering amplitude for this two-body problem in the presence of a Fermi sea and compute the vertex function  $V_{\mathbf{k}, \mathbf{k}'}$  describing pair-scattering processes  $(\mathbf{k}, -\mathbf{k}) \rightarrow (\mathbf{k}', -\mathbf{k}')$  that drive the pairing instability. We find that  $V_{\mathbf{k}, \mathbf{k}'}$  takes the form

$$V_{\mathbf{k}, \mathbf{k}'} = V_{\mathbf{k}, \mathbf{k}'}^{(0)} e^{i\frac{b}{2}e_z(\mathbf{k}' \times \mathbf{k})}, \quad (10)$$

factorizing into a real, cylindrically symmetric function  $V_{\mathbf{k}, \mathbf{k}'}^{(0)}$  and an angle-dependent phase factor, Eq. (18). The factor  $V_{\mathbf{k}, \mathbf{k}'}^{(0)}$  encodes the details of the two-body scattering potential, such as its strength and range, whereas the phase factor  $e^{i\frac{b}{2}e_z(\mathbf{k}' \times \mathbf{k})}$  encodes the geometric Berry phase acquired by Cooper pairs upon scattering and is universal, independent of microscopic details. This interaction leads to a chiral paired state described by

$$H = \sum_{\mathbf{k}} \xi_{\mathbf{k}} c_{\mathbf{k}}^\dagger c_{\mathbf{k}} + \sum_{\mathbf{k}} \Delta^*(\mathbf{k}) c_{-\mathbf{k}} c_{\mathbf{k}} + \Delta(\mathbf{k}) c_{\mathbf{k}}^\dagger c_{-\mathbf{k}}^\dagger. \quad (11)$$

The complex-valued  $\Delta(\mathbf{k})$  obeys the gap equation

$$\Delta(\mathbf{k}) = - \sum_{\mathbf{k}'} V_{\mathbf{k}, \mathbf{k}'} \frac{\Delta(\mathbf{k}')}{2E_{\mathbf{k}'}} \tanh \left( \frac{E_{\mathbf{k}'}}{2T} \right), \quad (12)$$

where  $E_{\mathbf{k}'} = \sqrt{|\Delta(\mathbf{k}')|^2 + \xi_{\mathbf{k}'}^2}$  and  $V_{\mathbf{k}, \mathbf{k}'}$  is the two-particle scattering amplitude due to the chiral interaction  $V(\mathbf{R}_1 - \mathbf{R}_2)$ . The angle dependence in  $V_{\mathbf{k}, \mathbf{k}'}$  will lead to an array of different chiral phases.

To understand the properties of  $V_{\mathbf{k}, \mathbf{k}'}$ , we consider the problem of two electrons scattering from the state  $(\mathbf{k}, -\mathbf{k})$  to the state  $(\mathbf{k}', -\mathbf{k}')$ . In the center-of-mass frame, Eq.(3), this process is governed by the scattering amplitude  $V_{\mathbf{k}, \mathbf{k}'} = \langle \mathbf{k} | \lambda e^{-a\hat{R}^2} | \mathbf{k}' \rangle$ . Working in the Landau gauge, we write the quantity  $\hat{R}^2$  as

$$\hat{R}^2 = (i\partial_{k_x} - bk_y)^2 - \partial_{k_y}^2. \quad (13)$$

Since  $x$  is conserved, we can use the Fourier transform

$$V_{\mathbf{k}, \mathbf{k}'} = \int dx e^{-i(k_x - k'_x)x} \tilde{V}_x(k_y, k'_y), \quad (14)$$

where  $\tilde{V}_x$  is a matrix element  $\langle k_y | e^{-a((x - bk_y)^2 - \partial_{k_y}^2)} | k'_y \rangle$ .

By making a substitution  $k_y \rightarrow k_y + \frac{x}{b}$ , we get  $\hat{R}^2 = b^2 k_y^2 - \partial_{k_y}^2$ . The matrix element  $\langle k_y | e^{-a(b^2 k_y^2 - \partial_{k_y}^2)} | k'_y \rangle$  can be calculated explicitly via 1D oscillator eigenstates

$$\langle k_y | e^{-a(b^2 k_y^2 - \partial_{k_y}^2)} | k'_y \rangle = \sqrt{\frac{2\pi b}{\sinh(2ab)}} \times \exp \left[ -\frac{b}{2\sinh(2ab)} ((k_y^2 + k_y'^2) \cosh(2ab) - 2k_y k_y') \right]. \quad (15)$$

Substituting back  $k_y \rightarrow k_y - \frac{x}{b}$  and integrating over  $x$ , we obtain the final answer

$$V_{\mathbf{k}, \mathbf{k}'} = \frac{\lambda\pi b}{\sinh(ab)} \exp \left[ -\frac{b}{4} \coth(ab) (\mathbf{k} - \mathbf{k}')^2 \right] \times \exp \left[ -i\frac{b}{2} (k_y + k_y')(k_x - k_x') \right]. \quad (16)$$

Importantly, the form of the vertex function depends on the choice of gauge  $\mathbf{a}(\mathbf{k})$ . To transform the result in the Landau gauge, Eq.(16), to the one in a symmetric gauge we perform a gauge transform for the electron wave functions,  $\mathbf{A} \rightarrow \mathbf{A} + \nabla f$ ,  $\psi \rightarrow \psi e^{if}$ . This yields

$$V_{\mathbf{k}, \mathbf{k}'} \rightarrow V_{\mathbf{k}, \mathbf{k}'} e^{if(\mathbf{k}) - if(\mathbf{k}')}. \quad (17)$$

By taking  $f(\mathbf{k}) = \frac{1}{2}bk_x k_y$ , we arrive at the answer in the symmetric gauge  $\mathbf{a} = \frac{1}{2}\mathbf{b} \times \mathbf{k}$ :

$$V_{\mathbf{k}, \mathbf{k}'} = \frac{\lambda\pi b}{\sinh(ab)} \exp \left[ -\frac{b}{4} \coth(ab) (\mathbf{k} - \mathbf{k}')^2 + i\frac{b}{2} e_z(\mathbf{k}' \times \mathbf{k}) \right] \quad (18)$$

where  $e_z(\mathbf{k}' \times \mathbf{k})$  denotes a scalar associated with the vector cross product pointing out of plane. As a sanity check, in the limit  $b \rightarrow 0$  we recover the vertex function familiar for short-range pairing interaction problem.

To isolate contributions to pairing with different angular momenta, we can project  $V_{\mathbf{k}, \mathbf{k}'}$  on the angular  $m$

harmonic on the Fermi surface. The angle dependence in  $V_{k,k'}$  is given by

$$V(\phi_k - \phi_{k'}) \sim \exp[A \cos(\phi_k - \phi_{k'}) + iB \sin(\phi_k - \phi_{k'})], \quad (19)$$

where  $A = \frac{b}{2} \coth(ab)k_F^2$ ,  $B = \frac{b}{2}k_F^2$ . Denoting  $u = \frac{A+B}{2}$ ,  $v = \frac{A-B}{2}$ , we can rewrite the last equation as

$$V(\phi_k - \phi_{k'}) \sim \exp[ue^{i(\phi_k - \phi_{k'})} + ve^{-i(\phi_k - \phi_{k'})}]. \quad (20)$$

We expand this expression in terms of angular harmonics

$$V(\phi) = \sum_m V_m e^{im\phi}, \quad V_m = \int \frac{d\phi}{2\pi} V(\phi) e^{-im\phi}. \quad (21)$$

The values  $V_m$  are readily obtained by inverse Fourier transform, giving a closed-form expression:

$$V_m = \frac{\lambda\pi b}{\sinh(ab)} e^{-\frac{bk_F^2}{2} \coth(ab)} I_m\left(\frac{bk_F^2}{2 \sinh(ab)}\right) e^{mab}. \quad (22)$$

The dependence of the quantities  $V_m$  on  $b$ ,  $k_F$  and parameter  $a$  characterizing the pair interaction potential width governs the hierarchy of the chiral states arising at different electron densities and Berry curvature values.

For a given pairing amplitude, the ground state is determined by  $V_m$  attaining the maximum value. By plotting these  $V_m$  for different values of  $k_F^2$  and  $b$ , we find that the channels  $m$  for which  $V_m$  is maximal alternate, leading to a cascade of transitions between phases with different  $m$  (see Fig. 1). Interestingly, this alternation pattern does not mimic the  $b$ -dependence of the two-particle bound states in Fig. 2, which shows no ground-state switching.

An interpretation of this oscillatory behavior can be obtained by focusing on the Berry curvature flux through the Fermi sea enclosed by the Fermi surface,

$$\Phi = \int_{FS} \mathbf{b} \frac{d^2k}{2\pi} = b \frac{k_F^2}{2}, \quad (23)$$

which is found to take approximately integer values at the phase boundaries. Indeed, the boundaries between adjacent phases  $m$  and  $m+2$  are determined by

$$I_m\left(\frac{\Phi}{\sinh(ab)}\right) = I_{m+2}\left(\frac{\Phi}{\sinh(ab)}\right) e^{2ab} \quad (24)$$

Using the asymptotics of the Bessel functions one can show that for the local attraction ( $a \rightarrow \infty$ ) the boundaries are determined by the equation  $\Phi = m+1$ , while for the wide potential ( $a \rightarrow 0$ ) the boundaries are given by small- $a$  asymptotics  $\Phi = \sqrt{(m+1)(m+2)}$ . These properties explain the behavior of different phases in the phase diagram shown in Fig. 1(b) at small and large  $ba$ .

We now consider the behavior near phase boundaries, the pairing interactions for the  $m$  and  $m+1$  orders are nearly equal, and they directly compete. On general symmetry grounds, at the phase boundaries these orders are

expected to exhibits a type-I phase transition. In this situation, the phase diagram typically contains two distinct superconducting phases, along with an intermediate region near the phase boundary where the two orders may coexist. Concretely, we focus on chiral superconducting pairing in the channels  $m$  and  $m+2$ , for which

$$\langle a_{\mathbf{k}} a_{-\mathbf{k}} \rangle \sim \Delta_1 e^{im\phi_{\mathbf{k}}} + \Delta_2 e^{i(m+2)\phi_{\mathbf{k}}}. \quad (25)$$

Within a mean-field framework, with an angle-dependent pairing interaction  $V_{\mathbf{k}\mathbf{k}'}$  that carries a geometric phase (as described above), this leads to the free energy

$$F(\Delta_1, \Delta_2) = -T \sum_{\mathbf{k}, i\omega_n} \text{Tr} \ln \begin{pmatrix} \epsilon_{\mathbf{k}} - i\omega_n & \Delta(\phi_{\mathbf{k}}) \\ \Delta^*(\phi_{\mathbf{k}}) & -\epsilon_{\mathbf{k}} - i\omega_n \end{pmatrix} + \frac{|\Delta_1|^2}{g_1} + \frac{|\Delta_2|^2}{g_2}, \quad g_1 = \nu V_m, \quad g_2 = \nu V_{m+2}, \quad (26)$$

where the gap function describes two competing pairing channels,  $\Delta(\phi_{\mathbf{k}}) = \Delta_1 e^{im\phi_{\mathbf{k}}} + \Delta_2 e^{i(m+2)\phi_{\mathbf{k}}}$ .

To obtain the dependence  $F(\Delta_1, \Delta_2)$ , we first carry out the (largely straightforward) summation over  $\omega_n$  and the radial integration over  $\mathbf{k}$  near the Fermi surface at fixed angle  $\phi_{\mathbf{k}}$ . Taking  $T = 0$  and, in the weak-coupling regime, assuming a small ratio  $\Delta/E_F \ll 1$ , this yields

$$F = \nu \oint \frac{d\phi_{\mathbf{k}}}{2\pi} |\Delta(\phi_{\mathbf{k}})|^2 \ln \frac{|\Delta(\phi_{\mathbf{k}})|^2}{E_F^2} + \frac{|\Delta_1|^2}{g_1} + \frac{|\Delta_2|^2}{g_2}, \quad (27)$$

This free energy, which can be evaluated analytically in closed form [58], captures the competition between chiral orders  $m$  and  $m+2$  and predicts first-order transitions at the phase boundaries.

The origin of the first-order transitions can be seen more clearly by considering the small- $a$  limit of the pairing interaction  $V(\mathbf{R}_{12}) = \lambda e^{-a(\mathbf{R}_1 - \mathbf{R}_2)^2}$ . When  $a \ll k_F^2$ , the interaction is wide-ranged in real space, which makes the Cooper pair scattering processes  $(\mathbf{k}, -\mathbf{k}) \rightarrow (\mathbf{k}', -\mathbf{k}')$  small-angle, i.e., nearly collinear. These processes, by connecting opposite patches on the Fermi circle, naturally lead to an angle-dependent superconducting order parameter  $\Delta(\theta)$  defined on the Fermi circle, with  $\theta$  the azimuthal angle. In this limit, superconductivity is effectively “patch-local,” and its behavior is described by a Ginzburg-Landau free energy that is local in  $\theta$ :

$$F(\Delta) = \int d\theta \frac{\kappa}{2} \bar{\Delta}(\theta) (i\partial_{\theta} - \Phi)^2 \Delta(\theta) - \alpha |\Delta|^2 + \frac{\beta}{2} |\Delta|^4, \quad (28)$$

where  $\Phi$  is the azimuthal component of Berry connection at the Fermi surface times  $k_F$ ,  $\Phi = \frac{1}{2}bk_F^2$ . Minimizing this free energy predicts states with  $2\pi m$  phase winding,  $\Delta(\theta) \sim e^{im\theta}$ , with energies varying with  $\Phi$  as

$$F_m(\Phi) \sim (m - \Phi)^2 |\Delta_0|^2 + F_m^{(0)}. \quad (29)$$

The  $m$  sectors are stable for  $m-1 < \Phi < m+1$ . For odd  $m$ , the phase boundaries at even integer  $\Phi$ , consistent with the small- $a$  phase diagram in Fig. 1(b).

A cascade of first-order transitions, which provides a clear experimental signature for this mechanism for chiral superconductivity, has several interesting implications:

One clear manifestation is oscillations of the critical temperature  $T_c$ , controlled by the Berry flux  $\Phi$  through the Fermi sea area and tunable via the carrier density. These oscillations are directly analogous to the Little–Parks effect in conventional superconductors in a magnetic field, where the periodicity of  $T_c$  as a function of flux allows one to measure the superconducting flux quantum  $hc/2e$ . In our case, the oscillations are governed by the commensurability of the flux  $\Phi$  through the Fermi sea and its area, realizing a quantum-geometry analog of the Little–Parks effect and providing a striking signature of chiral superconductivity.

Chiral superconducting phases with broken time-reversal symmetry are also expected to carry a finite magnetization. Estimating the orbital angular momentum per Cooper pair as  $hm$ , one finds a corresponding magnetic-moment density of order  $\mu_B m |\Delta|^2$ . The dependence of the magnetization on  $m$  manifests itself in the way an external magnetic field  $H$  reshapes the phase diagram. Specifically, the energy of a phase with angular momentum  $m$  is lowered by  $\sim \mu_B m |\Delta|^2 H$ , favoring phases with larger  $m$  and suppressing those with smaller  $m$ . As a result, in the presence of a field  $H$ , each phase

boundary in Fig. 1 is shifted inward (to smaller  $\Phi$ ) by an amount proportional to  $H$ .

Last but not least, in a spatially nonuniform system, first-order transitions between phases with different  $m$  will generate domains separated by boundaries that host chiral edge modes. The edge supercurrents carried by these modes can be directly probed by spatially resolved scanning magnetometry, while the chiral quasiparticles localized at the domain walls can be detected through signatures in chiral thermal transport.

In summary, this work demonstrates that Berry curvature in electronic bands qualitatively reshapes the superconducting pairing problem, giving rise to a cascade of chiral superconducting states characterized by quantized angular momentum  $m$ . Unlike conventional vortex physics driven by real-space magnetic fields, the Berry-curvature-induced pseudomagnetic field acts in  $k$  space, modifying the microscopic structure of Cooper pairs. As a result, superconducting order parameters acquire intrinsic phase winding on the Fermi surface, leading to a family of topologically distinct chiral states, manifested in a number of signatures readily detectable by state-of-the-art experimental techniques.

This work greatly benefited from discussions with Patrick Lee, Brian Skinner and Eli Zeldov.

---

[1] Bruno Uchoa and A. H. Castro Neto, “Superconducting states of pure and doped graphene,” *Phys. Rev. Lett.* **98**, 146801 (2007).

[2] A. M. Black-Schaffer and S. Doniach, “Resonating valence bonds and mean-field d-wave superconductivity in graphite,” *Phys. Rev. B* **75**, 134512 (2007).

[3] Carsten Honerkamp, “Density waves and Cooper pairing on the honeycomb lattice,” *Phys. Rev. Lett.* **100**, 146404 (2008).

[4] Sandeep Pathak, Vijay B. Shenoy, and G. Baskaran, “Possible high-temperature superconducting state with a d+id pairing symmetry in doped graphene,” *Phys. Rev. B* **81**, 085431 (2010).

[5] R. Nandkishore, L. S. Levitov, and A. V. Chubukov, “Chiral superconductivity from repulsive interactions in doped graphene,” *Nat. Phys.* **8**, 158–163 (2012).

[6] Maximilian L. Kiesel, Christian Platt, Werner Hanke, Dmitry A. Abanin, and Ronny Thomale, “Competing many-body instabilities and unconventional superconductivity in graphene,” *Phys. Rev. B* **86**, 020507 (2012).

[7] Y. Cao, V. Fatemi, S. Fang, K. Watanabe, T. Taniguchi, E. Kaxiras, and P. Jarillo-Herrero, “Unconventional superconductivity in magic-angle graphene superlattices,” *Nature* **556**, 43–50 (2018).

[8] M. Yankowitz, S. Chen, H. Polshyn, Y. Zhang, K. Watanabe, T. Taniguchi, D. Graf, A. F. Young, and C. R. Dean, “Tuning superconductivity in twisted bilayer graphene,” *Science* **363**, 1059–1064 (2019).

[9] X. Lu, P. Stepanov, W. Yang, M. Xie, M. A. Aamir, I. Das, C. Urgell, K. Watanabe, T. Taniguchi, G. Zhang, A. Bachtold, A. H. MacDonald, and D. K. Efetov, “Superconductors, orbital magnets and correlated states in magic-angle bilayer graphene,” *Nature* **574**, 653–657 (2019).

[10] G. Chen, A. L. Sharpe, P. Gallagher, I. T. Rosen, E. J. Fox, L. Jiang, B. Lyu, H. Li, K. Watanabe, T. Taniguchi, J. Jung, Z. Shi, D. Goldhaber-Gordon, Y. Zhang, and F. Wang, “Signatures of tunable superconductivity in a trilayer graphene moiré superlattice,” *Nature* **572**, 215–219 (2019).

[11] P. Stepanov, I. Das, X. Lu, A. Fahimniya, K. Watanabe, T. Taniguchi, F. H. L. Koppens, J. Lischner, L. Levitov, and D. K. Efetov, “Untying the insulating and superconducting orders in magic-angle graphene,” *Nature* **583**, 375–378 (2020).

[12] H. Zhou, L. Holleis, Y. Saito, L. Cohen, W. Huynh, C. L. Patterson, F. Yang, T. Taniguchi, K. Watanabe, and A. F. Young, “Isospin magnetism and spin-polarized superconductivity in Bernal bilayer graphene,” *Science* **375**, 774–778 (2022).

[13] B. Uchoa and Y. Barlas, “Superconducting states in pseudo-Landau-levels of strained graphene,” *Phys. Rev. Lett.* **111**, 046604 (2013).

[14] Y. Choi *et al.*, “Superconductivity and quantized anomalous Hall effect in rhombohedral graphene,” *Nature* **639**, 342–347 (2025).

[15] H. Zhou *et al.*, “Superconductivity in rhombohedral trilayer graphene,” *Nature* **598**, 434–438 (2021).

[16] Y. Guo *et al.*, “Flat band surface state superconductivity in thick rhombohedral graphene,” arXiv:2511.17423 [cond-mat.supr-con] (2025).

[17] M. Kumar *et al.*, “Superconductivity from dual-surface

carriers in rhombohedral graphene,” arXiv:2507.18598 [cond-mat.mes-hall] (2025).

[18] J. Xie *et al.*, “Magnetic-Field-Driven Insulator-Superconductor Transition in Rhombohedral Graphene,” arXiv:2512.24306 [cond-mat.supr-con] (2025).

[19] C. L. Patterson *et al.*, “Superconductivity and spin canting in spin-orbit proximitized rhombohedral trilayer graphene,” *Nature* **641**, 632–638 (2025).

[20] J. Yang *et al.*, “Impact of spin-orbit coupling on superconductivity in rhombohedral graphene,” *Nat. Mater.* **24**, 1058–1065 (2025).

[21] T. Han *et al.*, “Orbital multiferroicity in pentalayer rhombohedral graphene,” *Nature* **623**, 41–47 (2023).

[22] H. Zhou *et al.*, “Isospin magnetism and spin-polarized superconductivity in Bernal bilayer graphene,” *Science* **375**, 774–778 (2022).

[23] C. Li *et al.*, “Tunable superconductivity in electron- and hole-doped Bernal bilayer graphene,” *Nature* **631**, 300–306 (2024).

[24] L. Holleis *et al.*, “Nematicity and orbital depairing in superconducting Bernal bilayer graphene,” *Nat. Phys.* **21** (2025),

[25] T. Han, Z. Lu, Z. Hadjri, L. Shi, Z. Wu, W. Xu, Y. Yao, A. A. Cotten, O. Sharifi Sedeh, H. Weldeyesus, J. Yang, J. Seo, S. Ye, M. Zhou, H. Liu, G. Shi, Z. Hua, K. Watanabe, T. Taniguchi, P. Xiong, D. M. Zumbühl, L. Fu, and L. Ju, “Signatures of chiral superconductivity in rhombohedral graphene,” *Nature* **643**, 654–661 (2025),

[26] M. Tinkham, *Introduction to Superconductivity*, 2nd ed. (McGraw-Hill, New York, 1996).

[27] E. H. Brandt, “The flux-line lattice in superconductors,” *Rep. Prog. Phys.* **58**, 1465–1594 (1995).

[28] G. Blatter, M. V. Feigel’man, V. B. Geshkenbein, A. I. Larkin, and V. M. Vinokur, “Vortices in high-temperature superconductors,” *Rev. Mod. Phys.* **66**, 1125–1388 (1994).

[29] G. W. Crabtree and D. R. Nelson, “Vortex physics in high-temperature superconductors,” *Phys. Today* **50**(4), 38–45 (1997).

[30] W.-K. Kwok, U. Welp, A. Glatz, A. E. Koshelev, K. J. Kihlstrom, and G. W. Crabtree, “Vortices in high-performance high-temperature superconductors,” *Rep. Prog. Phys.* **79**, 116501 (2016).

[31] G. Sundaram and Q. Niu, *Phys. Rev. B* **59**, 14915 (1999).

[32] D. Xiao, M.-C. Chang, and Q. Niu, *Rev. Mod. Phys.* **82**, 1959 (2010).

[33] G. Panati, H. Spohn, and S. Teufel, *Commun. Math. Phys.* **242**, 547 (2003).

[34] S. Teufel, *Adiabatic Perturbation Theory in Quantum Dynamics* (Springer, 2003).

[35] S. A. Murshed and B. Roy, “Nodal pair density waves from a quarter-metal in crystalline graphene multilayers,” *Phys. Rev. B* **112**, 085121 (2025).

[36] Y.-Z. Chou, J. Zhu, and S. Das Sarma, “Intravalley spin-polarized superconductivity in rhombohedral tetralayer graphene,” *Phys. Rev. B* **111**, 174523 (2025).

[37] G. Parra-Martinez, A. Jimeno-Pozo, V. T. Phong, H. Sainz-Cruz, D. Kaplan, Peleg Emanuel, Yuval Oreg, Pierre A. Pantaleon, J. A. Silva-Guillen, and F. Guinea, “Band Renormalization, Quarter Metals, and Chiral Superconductivity in Rhombohedral Tetralayer Graphene,” *Phys. Rev. Lett.* **135**, 136503 (2025).

[38] H. Yang and Y.-H. Zhang, “Topological incommensurate Fulde-Ferrell-Larkin-Ovchinnikov superconductor and Bogoliubov Fermi surface in rhombohedral tetralayer graphene,” arXiv:2411.02503 (2024).

[39] Q. Qin and C. Wu, “Chiral finite-momentum superconductivity in the tetralayer graphene,” arXiv:2412.07145 (2024).

[40] G. Shavit and J. Alicea, “Quantum Geometric Kohn-Luttinger Superconductivity,” *Phys. Rev. Lett.* **134**, 176001 (2025).

[41] M. Geier, M. Davydova, and L. Fu, “Chiral and topological superconductivity in isospin polarized multilayer graphene,” arXiv:2409.13829 (2024).

[42] A. Jahin and S.-Z. Lin, “Enhanced Kohn-Luttinger topological superconductivity in bands with nontrivial geometry,” arXiv:2411.09664 (2024).

[43] D. Guerci, A. Abouelkomsan, and L. Fu, “From Fractionalization to Chiral Topological Superconductivity in a Flat Chern Band,” arXiv:2506.10938 (2025).

[44] Z. Dong, A. S. Patri, and T. Senthil, “Stability of Anomalous Hall Crystals in multilayer rhombohedral graphene,” *Phys. Rev. B* **110**, 205130 (2024).

[45] J. May-Mann, T. Helbig, and T. Devakul, “How pairing mechanism dictates topology in valley-polarized superconductors with Berry curvature,” arXiv:2503.05697 (2025).

[46] Z. Wang, L. Dong, C. Xiao, and Q. Niu, “Berry curvature effects on quasiparticle dynamics in superconductors,” *Phys. Rev. Lett.* **126**, 187001 (2021).

[47] O. Matsyshyn, G. Vignale, and J. C. W. Song, “Superconducting Berry curvature dipole,” arXiv:2410.21363 (2024).

[48] A. Ghazaryan, T. Holder, E. Berg, and M. Serbyn, “Multilayer graphenes as a platform for interaction-driven physics and topological superconductivity,” *Phys. Rev. B* **107**, 104502 (2023).

[49] A. Jahin and S.-Z. Lin, “Enhanced Kohn-Luttinger superconductivity in geometric bands,” *Phys. Rev. B* **113**, 014504 (2026).

[50] E. Viñas Boström, A. Fischer, J. B. Profe, J. Zhang, D. M. Kennes, and A. Rubio, “Phonon-mediated unconventional *s*- and *f*-wave pairing superconductivity in rhombohedral stacked multilayer graphene,” *npj Comput. Mater.* **10**, 163 (2024).

[51] F. Gaggioli, D. Guerci, and L. Fu, “Spontaneous vortex-antivortex lattice and Majorana fermions in rhombohedral graphene,” *Phys. Rev. Lett.* **135**, 116001 (2025).

[52] F. Paoletti, D. Guerci, G. Sangiovanni, U. F. P. Seifert, and E. J. König, “Topologically enabled superconductivity: possible implications for rhombohedral graphene,” arXiv:2504.13166 (2025).

[53] M. Sato and Y. Ando, “Topological superconductors: a review,” *Rep. Prog. Phys.* **80**, 076501 (2017).

[54] C. Kallin and J. Berlinsky, “Chiral superconductors,” *Rep. Prog. Phys.* **79**, 054502 (2016).

[55] N. Read and D. Green, “Paired states of fermions in two dimensions with breaking of parity and time-reversal symmetries and the fractional quantum Hall effect,” *Phys. Rev. B* **61**, 10267–10297 (2000).

[56] C. Nayak, S. H. Simon, A. Stern, M. Freedman, and S. Das Sarma, “Non-Abelian anyons and topological quantum computation,” *Rev. Mod. Phys.* **80**, 1083–1159 (2008).

[57] T. Han *et al.*, “Signatures of chiral superconductivity in rhombohedral graphene,” *Nature* (2025),

[58] Integration over the angle  $\phi_k$  can be carried out using

the identity

$$\int_0^{2\pi} |a + be^{i\phi}|^2 \ln(|a + be^{i\phi}|^2) \frac{d\phi}{2\pi} = (30)$$

$$(|a|^2 + |b|^2) (1 + \ln \max(|a|^2, |b|^2)) - | |a|^2 - |b|^2 |.$$